

Numerical Study of the Stress Response of Two-Dimensional Dense Granular Packings

N. Gland, P. Wang and H. A. Makse
Levich Institute and Physics Department
City College of New York, New York, NY 10031

We investigate the Green function of two-dimensional dense random packings of grains in order to discriminate between the different theories of stress transmission in granular materials. Our computer simulations allow for a detailed quantitative investigation of the dynamics which is difficult to obtain experimentally. We show that both hyperbolic and parabolic models of stress transmission fail to predict the correct stress distribution in studied region of the parameters space. We demonstrate that the compressional and shear components of the stress compare very well with the predictions of isotropic elasticity for a wide range of pressures and porosities and for both frictional and frictionless packings. However, the pressures used in this study do not include the critical isotropic point, so that our results do not preclude the fact that corrections to elasticity may appear at the critical point of jamming. We show that the agreement holds in the bulk of the packings as well as at the boundaries and we validate the linear dependence of the stress profile width with depth.

PACS numbers: 81.05.Rm, 81.40.Jj

I. INTRODUCTION

The theoretical understanding of the structural and mechanical properties of static granular assemblies is still an open issue [1]. Indeed, there is no consensus on how the stress distribution should be expressed and how granular materials respond to applied perturbations. Experimental measurements of stress distributions in silos and sandpiles [2, 3, 4, 5] seem to be incompatible with a simple elastic theory and have led to the development of new mechanical formulations for granular matter where new assumptions are proposed [6, 7].

The equations of equilibrium for the stress tensor, σ_{ij} , are

$$\vec{\nabla} \cdot \vec{\sigma} = \rho \vec{g}, \quad (1)$$

where ρ is the density of the medium and \vec{g} the gravitational acceleration vector. From this equation we see that the stress is indeterminate. For instance in 2D, it provides two independent equations for the three components of the stress tensor (the stress tensor is symmetrical, $\sigma_{xy} = \sigma_{yx}$). Thus a third constitutive equation (the missing equation) characterizing the behavior of the material is needed in order to provide closure to the problem. In the elastic formulation closure is provided by the introduction of the strain field and new constitutive relations relating the strain with the strain (Hooke's law). This leads to elliptic equations governing the stress distribution [8].

Unlike elasticity— where the closure is provided by Hooke's law— new granular models propose closure relations involving only stress tensor components [6]. Hyperbolic equations of the same mathematical structure as a wave equation are thus obtained. As a consequence, a load applied at the surface propagates along two characteristic directions.

Another theoretical framework of stress transmission

in granular matter (the q-model) was introduced by Copersmith *et al.* [7]. It considers the transmission of interparticle forces by a random redistribution of forces among nearest neighbors. At the continuum scale [9], the stress components satisfy a parabolic equation of diffusion, expected from the stochastic uncorrelated nature of the transmission process.

Thus, different theories predict different stress distributions according to the nature of the equations governing the stress. The importance of resolving which of these models apply under which circumstances is of major theoretical and practical interest in order to reveal the real mechanical properties of static granular assemblies.

In order to test the validity of the different models, a simple experiment was proposed by de Gennes [10]: the calculation of the Green function by applying a perturbation force on a grain in the granular medium and measuring the resulting stress field perturbation. The elastic and the new models predictions are then confronted. In the most simple case of an homogeneous isotropic material, the elastic framework predicts that the vertical stress profile resulting from the perturbation is a single peak centered below the perturbation with a width W proportional to the depth y from the perturbation. In the hyperbolic models, the stress profile presents a distinctive double peak and in the parabolic models the profile is a single peak as in the elastic prediction but with a width proportional to $W \sim \sqrt{y}$.

The Green function experiment has been recently performed by several groups. The work of Reydellet and Clement [11] and Geng *et al.* [12] show a single peak in the stress distribution in σ_{yy} in qualitative agreement with the elastic framework. However, other experiments show qualitative agreement with the diffusion models of stress transmission [13]. Under some circumstances, the two peaks in the stress characteristic of the hyperbolic models have been also observed [14, 15, 16, 17, 18, 19]. Also, it was shown that the de-

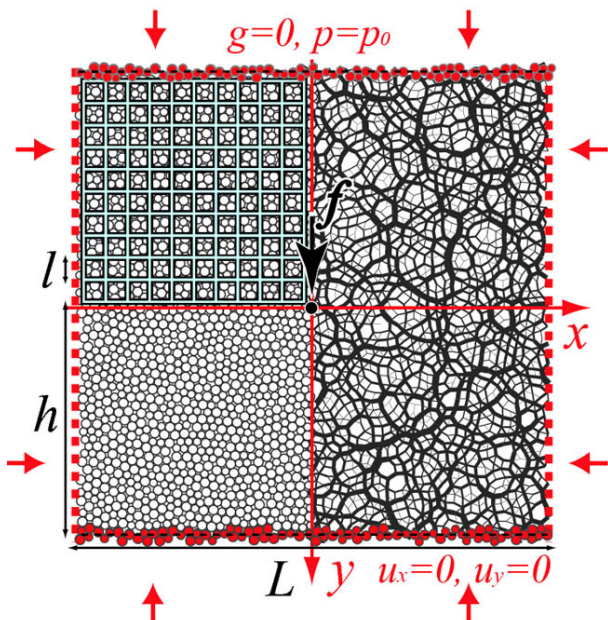


FIG. 1: System geometry. The left part of the figure shows a detail of the bidisperse particle packing and the typical grid used to calculate the coarse-grained stress profile, while the right part shows the heterogeneity in the interparticle forces (“force chains”). A small force f is applied on a single grain located at the center of the sample (origin of reference axes). The vertical boundaries are composed of rigid grains while the horizontal boundaries are periodic.

gree of ordering [20, 21, 22, 23] and the texture properties of packings [25] affect strongly the stress transmission. Even though, there is general consensus that the elastic theory may describe qualitatively the system, many discrepancies still remain [24]. A microscopic study is needed to perform a *quantitative* assessment of the validity of the different theoretical approaches. Simulations offer an optimum scenario to compare the different theories and allow to obtain microscopic information [25, 26] and the exact system dynamics [27], difficult to observe in experiments.

Here we perform MD simulations to gain more microscopic insight into the mechanical response of granular matter. Our results indicate that the elastic theory can describe the simulations better than the other models. Indeed, we find a stress response whose vertical component shows one peak. Furthermore we show that elasticity predicts very accurately all components of the stress tensor at all depths in the packing, for all the ranges of pressures, porosities and frictional properties studied in this work.

II. NUMERICAL SIMULATIONS.

We developed a numerical code based on the Discrete Element Method (DEM). The model deals with an assembly of elastic spheres interacting via the Hertz-

Mindlin contact laws. The grains interact with one another via non-linear Hertz normal forces f_n^c which depend on the overlap between two spheres, and frictional transverse forces f_t^c which depend both on the shear and normal displacements between the grains:

$$\begin{aligned} f_n^c &= \frac{2}{3} C_n R^{1/2} w^{3/2}, \\ \Delta f_t^c &= C_t (Rw)^{1/2} \Delta s, \end{aligned} \quad (2)$$

where $R = 2R_1R_2/(R_1 + R_2)$ with R_1 and R_2 the radii of the spheres in contact. The normal overlap between the two grain is w , and Δs is the relative shear displacement between the two grain centers. The constants $C_n = 4G/(1-\nu)$ and $C_t = 4G/(2-\nu)$ are defined in terms of the shear modulus $G = 29\text{GPa}$ and the Poisson’s ratio $\nu = 0.2$ of the material of the grains. Coulomb friction, $f_t^c \leq \mu_f f_n^c$, [28] is also included in the model and we set the friction coefficient $\mu_f = 0.3$. We also include viscous damping terms in the equations of motions (translational and rotational) to allow the system to relax toward static equilibrium. In this study, the grains spherical are constrained to move in 2D.

The packings are prepared using binary mixtures of particles at equal concentrations characterized by a radius $R = (0.1 \pm 0.01)\text{mm}$ in order to avoid crystallization. We study different sample sizes ranging from $N = 10000$ to $N = 250000$ particles equilibrated using periodic boundary conditions in the horizontal directions and two rigid walls made of grains at the top and the bottom of the system (see Fig. 1). In order to prepare the larger samples at static equilibrium and ‘save’ computational time on the preparation procedure, we repeated periodically in space the smaller sample equilibrated using periodic boundaries conditions in both horizontal and vertical directions. We use a numerical compaction protocol designed to prepare confined dense granular isotropic packings explained in detail in [29]. We set the gravity $\vec{g} = \vec{0}$ since the pressures of confinement considered in this work are sufficiently high.

During the preparation, the friction at the contacts is turned off and the system is able to reach a dense isotropic state with no dependence on the “history” of preparation. We check the isotropy and randomness of the packings by calculating both the texture tensor and the 2D orientational order parameter [30]. In a first part, the simulated granular aggregates are prepared with target pressure of 2.10^3 N/m (equivalent to a pressure of 10MPa in 3D) and result with an average coordination number $Z \approx 4.3$ compared to the isostatic limit $Z = 4$ [31], and a solid volume fraction $\phi \approx 0.85$ slightly above the random close packing limit of $\phi \approx 0.82$. In a next part we show results for lower pressures 2.10^1 N/m and 2.10^2 N/m (equivalent to 100KPa and 1MPa) with $Z \approx 4.1$ and $\phi \approx 0.83$, in order to be closer to the isostatic point. The next step of the preparation protocol consists to break the vertical symmetry of the system by removing the periodic conditions in the vertical direction and replacing it by rigid walls made of rough particles at this time, we

also restore the friction $\mu_f = 0.3$ in the system.

Next, we select the particle nearest to the center of the system and apply a vertical downward force. The amplitude of the force, $f = 10^{-6}\langle f \rangle$ (where $\langle f \rangle$ is the average normal force in the packing), is small enough to assure that we measure the linear response regime. To calculate the local stress tensor $\sigma_{ij}(x, y)$, the system is subdivided into square cells of size $l = 0.5$ mm containing about 4 to 5 particles depending on their local arrangements (see upper left corner of Fig. 1). The results are independent of the size of the coarse-graining cell in the range l to $3l$.

We have performed these simulations using three different system sizes in a range L to $3L$ in order to find the minimal size to consider to avoid finite size effects. The aspect ratio 1 to 3 is needed for the appropriate study of the stress response function because the width is of the order of y . We find that the vertical response is less sensitive than the two others component to the sample size. We have also compared the vertical response functions above and below the perturbation, respectively in the dilatation region and in the compression region. We find an horizontal symmetry $\sigma_{ii}(x, y) \approx \sigma_{ii}(x, -y)$, showing that the compression response and the dilatation response are almost identical in the studied linear regime.

We measure (x, y) in units of l with $x = 0, y = 0$ at the center of the packing. We consider system sizes ranging from $L = 40l$ ($N = 10000$) to $L = 120l$ ($N = 90000$). We find no appreciable size effects in this range for $\sigma_{yy}(x, y)$ and slight size effects for $\sigma_{xx}(x, y)$ and $\sigma_{xy}(x, y)$ saturating above $L = 80l$ ($N = 40000$). The perturbation of the stress is calculated as $\sigma_{ij} = \sigma_{ij}^{per} - \sigma_{ij}^{ref}$, where σ_{ij}^{ref} is the stress of the initial reference state before the perturbation and σ_{ij}^{per} is the stress after the perturbation is applied ($\sigma_{ii} > 0$ corresponds to compression). Because of the discrete nature of the material and the strong inhomogeneity of the contact network [30] (see Fig. 1), we average the stress response functions over many configurations of particles (about 20).

III. STRESS DISTRIBUTION.

The application of the force on the central particle generates a pressure wave which propagates in the granular packing (as seen in the inset of Fig. 2a) and is reflected at the rigid and periodic boundaries. The wave is dissipated slowly over time until the packing reaches a new static state at mechanical equilibrium. Figure 2a presents the evolution with time of the vertical stress $\sigma_{yy}(x = 1, y, t > 0)$ at different depths y below the perturbation in the compression region. At all depths, a first stress maximum is observed at the passage of the front wave (local instantaneous response in the propagative regime, point A), followed by a rapid oscillation and then a slow relaxation (point B). Then, a new stress peak of smaller amplitude is measured (point A') which corresponds to the wave reflected at the boundary followed by the same decrease sequence towards complete relaxation

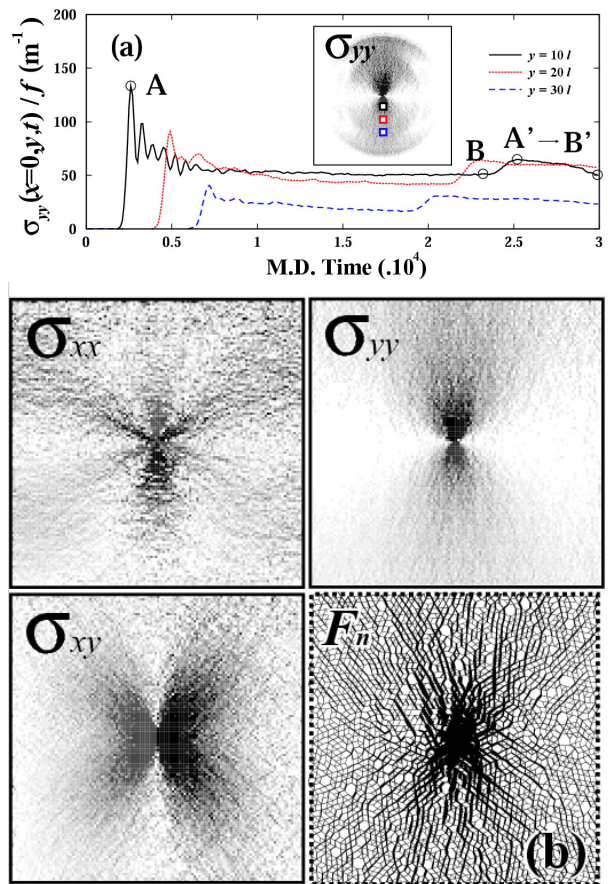


FIG. 2: (a) Time evolution of σ_{yy} in a single frictional packing at $x = 0$ and at four different depths y (as indicated by the squares in the inset, showing the stress propagation). We observe an instantaneous stress peak (point A) in the propagative regime as a result of the wave front first passage followed by a relaxation to point B to the static regime and a subsequent peak followed by another relaxation (from A' to B'). The slow damping drives the system from a propagative regime to a static state. (b) Typical stress response functions of one packing for the three components of the stress tensor σ_{xx} , σ_{yy} and σ_{xy} and the enlarged detail of the perturbation of the normal forces F_n on the contact network shown in Fig. 1.

to the new static state (point B'). The further the point of measurement is, the smaller is the amplitude of the first stress maximum resulting from the expansion of the front.

Figure 2b plots the stresses at equilibrium as well as the perturbation of the normal interparticle forces, F_n . We clearly see the existence of a single peak in σ_{yy} in agreement with elasticity and the experiments of [11, 12] and in disagreement with the predictions of the hyperbolic theories of stress transmission.

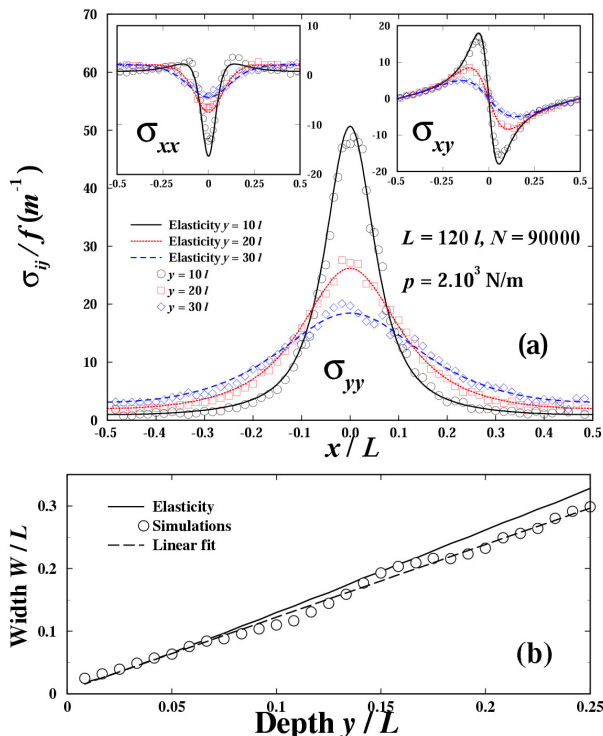


FIG. 3: (a) Comparison between the solutions for the stress between simulations (symbols) and elasticity (lines) at different depths y and at a fixed pressure. The main plot compares the vertical component of the stress tensor σ_{yy} while the insets compare the two others components σ_{xx} and σ_{xy} . (b) Half-width amplitude of the averaged vertical stress profiles with increasing depth. A linear dependence is $W \sim 1.15y$ is found, corroborating the elastic solution $W \sim 1.30y$.

IV. COMPARISON WITH ELASTICITY.

Next, we make a detailed comparison with the prediction of elasticity theory. In the case of an infinite elastic medium the solution was calculated by Boussinesq [28]:

$$\sigma_{yy}(x, y) = \frac{2}{\pi} \frac{f}{y} \frac{1}{\left(1 + \left(\frac{x}{y}\right)^2\right)^2}. \quad (3)$$

However, there is no analytical solution for the boundary conditions used in the present part of the study, i.e., rigid top and bottom rough boundaries where the strain satisfies $u_y(x, y = \pm L/2) = 0$, and $u_x(x, y = \pm L/2) = 0$ (this conditions can be expressed in terms of the stress tensor as $\partial_y \sigma_{xx}(x, y = \pm L/2) = (2 + \nu) \partial_x \sigma_{xy}(x, y = \pm L/2)$ and $\sigma_{xx}(x, y = \pm L/2) = \nu \sigma_{yy}(x, y = \pm L/2)$ respectively, where ν is the Poisson's coefficient of the entire packing [24]) and horizontal periodic boundary conditions. Then, we find the solution of Eq. (1) numerically [32]. The applied perturbation $Q(x)$ is taken to be a narrow Gaussian centered at $x = 0, y = 0$, such that $\sigma_{yy}(x, y = 0, t > 0) = Q(x)$. In the theory, we set the Poisson's coefficient for the entire system to $\nu = 0.28$ according to simulations and experiments [29]. Figure

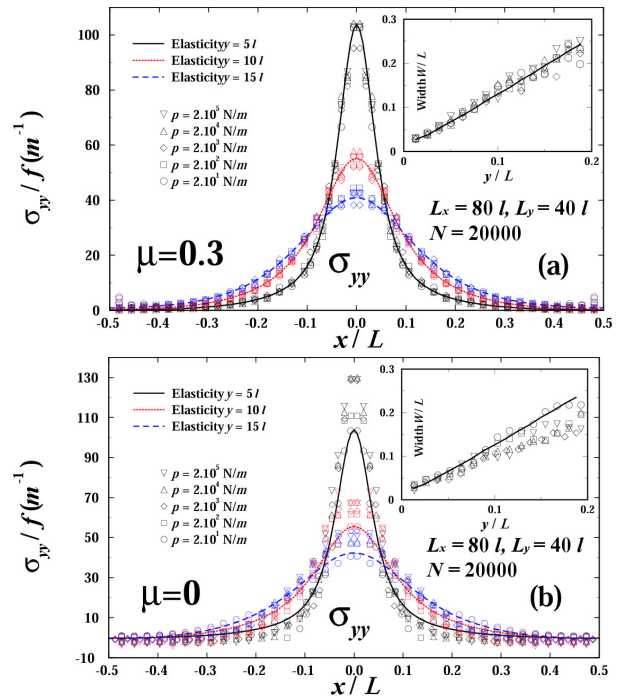


FIG. 4: Comparison between the vertical stress prediction of elasticity and the simulations at different pressures ranging from $p = 2.10^1 N/m$ to $p = 2.10^5 N/m$ for (a) rough boundaries conditions / frictional particles, (b) smooth boundaries conditions / frictionless particles. The insets show the half-width amplitude of the corresponding stress profiles with increasing depth. Linear dependence $W \sim y$ is found.

3a shows how the elastic solution compares with the numerical results for the stress components. The elastic solution provides a very satisfactory fit at all depth for all the components of the stress tensor.

Width of the Stress Profile.— We obtain the width of the vertical stress profile as a function of the depth y by calculating the half-amplitude spread of the distribution [11]. Figure 3b shows a linear dependence on the depth, $W \sim y$, in general agreement with elasticity (and in disagreement with the parabolic model [7]). The numerical response ($W = 1.15y$) exhibits a slightly narrower response than the elastic solution ($W = 1.30y$); it was also found in experiments [11] and could be attributed to the disorder of the packing.

Pressure and Friction Effects.— We also study the stress response functions for different pressures (from $p = 2.10^1 N/m$ to $p = 2.10^5 N/m$) and porosities on smaller systems ($L = 80l$ and $N = 20000$) shown in Fig. 4a. We find that the stress profiles averaged over 20 realizations are in extremely good agreement with the elastic prediction for rough boundaries. Moreover the profiles do not show appreciable pressure dependence. This is in further agreement with elasticity. Indeed the elastic solution depends only on the Poisson ratio ν which is constant with pressure [29]. Moreover, we find the same

linear dependence with the depth ($W = 1.20y$) for the studied range of pressure (see inset of Fig. 4a). The agreement with elasticity holds very well also for the two others components.

We also investigate the effect of friction by performing simulations with frictionless packings ($\mu_f = 0$) in the same range of pressure and with the same system size shown in Fig. 4b. This time, we compare the stress profiles averaged over 50 realizations (due to much larger fluctuations) with the elastic prediction for smooth boundaries (i.e., $\sigma_{xy}(x, y = \pm L/2) = 0$). We find that the stress profiles show a small pressure dependence and that the agreement with the elastic prediction holds better for the smallest pressure. The reason for the discrepancy could come from the fact that even though the particles are frictionless, the fixed grains at the top and bottom surface induce a roughness, the effect of which is expected to be more important at high pressures. Indeed despite non-frictional particles, a non-zero shear stress is found at the boundary, whose amplitude increases with pressure. The linear dependence of the half-amplitude show similar dependence with pressure.

V. SUMMARY

Our numerical work shows that, for the studied frictional and frictionless packings, the vertical component of the stress response has a single peak at all depths and that the half-amplitude width of the vertical stress profiles is proportional to the depth. By calculating the stress profiles using the elasticity framework and taking into account the exact geometry of the simulations,

we compare the numerical results and find very good agreement with elasticity for the three components of the stress tensor in the frictional case. Whereas, experiments probe only the vertical stress profile at the boundary, our numerical simulations are able to show the agreement with elasticity at all depth inside the packings and all the components. Furthermore, we confirm that pressure is not a critical parameter for the stress response function of frictional packings.

However, it is important to note that the system may not be close enough to the isostatic point to show critical behavior and a deviation from the elastic solution. Thus, we may still expect corrections to appear if the system is prepared closer to the isostatic jamming point $Z_c = 4$. It will be of interest, then, to continue this work and investigate the critical regime as well. We also demonstrate that the response of frictionless packings is consistent with elasticity; it exhibits pressure dependency and tends to agree with elasticity at low pressure. We attribute this effect to the roughness of the boundaries in our simulations. In further work, it would be interesting to confront the more general anisotropic elastic theory to the response of loose and anisotropic packings obtained by other compaction protocols.

Acknowledgments

We thank P. Claudin, E. Clement, Y. Gueguen, D. L. Johnson, E. Kolb, D. Pisarenko and C. Song for stimulating discussions. This work has been supported by the Department of Energy and the National Science Foundation.

-
- [1] Mehta A. and Halsey T. C., *Proceedings of the Workshop "Challenges in Granular Physics" Adv. Complex Syst.*, **4** (2001) 287.
 - [2] Smid J. and Novosad J., *Proc. Powtech. Conference 1981, Ind. Chem. Eng. Symp.*, **63**, D3V1 (1981).
 - [3] Brockbank R., Huntley J. M., and Ball R. C., *J. Phys. II (France)*, **7** (1997) 1521.
 - [4] Vanel L. *et al.*, *Phys. Rev. E*, **60** (1999) R5040.
 - [5] Vanel L. *et al.*, *Phys. Rev. Lett.*, **84** (2000) 1439.
 - [6] Bouchaud J.-P., Cates M. E., and Claudin P., *J. Phys. I (France)*, **5** (1995) 639.
 - [7] Coppersmith S. N. *et al.*, *Phys. Rev. E.*, **53** (1996) 4673.
 - [8] Landau L. D. and Lifshitz E. M., *The Theory of Elasticity* (Pergamon, Oxford) 1970.
 - [9] Claudin P. *et al.*, *Phys. Rev. E*, **57** (1998) 4441.
 - [10] De Gennes P. G., *Rev. Mod. Phys.*, **71** (1999) 374.
 - [11] Reydellet G. and Clement E., *Phys. Rev. Lett.*, **86** (2001) 3308.
 - [12] Geng J. *et al.*, *Phys. Rev. Lett.*, **87** (2001) 035506.
 - [13] Da Silva M. and Rajchenbach J., *Nature*, **406** (2000) 708.
 - [14] Geng J. *et al.*, *Physica D*, **182** (2003) 274.
 - [15] Head D. A. *et al.*, *Eur. Phys. J. E*, **6** (2001) 99.
 - [16] Breton L. *et al.* *Europhys. Lett.* **60** (2002) 813.
 - [17] Silveira *et al.* cond-mat 0208214 (2002).
 - [18] Moukarzel C. F. *et al.* *Granular Matter*, **6**, 61 (2004).
 - [19] Goldhirsch I. and Goldenberg C. *Phys. Rev. Lett.* **89**, 084302 (2002).
 - [20] Mueggenburg N. W. *et al.* *Phys. Rev. E* **66** 2002 031304.
 - [21] Spanauth M. J. *et al.* cond-mat 0308580 (2003).
 - [22] Bonamy D. *et al.* *Phys. Rev. E* **68**, 042301 (2003).
 - [23] Otto M. *et al.* *Phys. Rev. E* **67**, 031302 (2003).
 - [24] Serero D. *et al.* *Eur. Phys. J. E* **6**, 169 (2001).
 - [25] Atman A. P. F. and Claudin P. *cond-mat* 0310564 (2003).
 - [26] Silbert L. E. *et al.* *Phys. Rev. E* **66**, 061303 (2002).
 - [27] Somfai E. *et al.* *cond-mat* 0408128 (2004).
 - [28] Johnson K. L., *Contact Mechanics*, (Cambridge University Press) 1985.
 - [29] H. A. Makse, N. Gland, D. L. Johnson, and L. M. Schwartz, *Phys. Rev. E* **70**, 061302 (2004).
 - [30] Radjai F. *et al.*, *Phys. Rev. Lett.*, **77** (1996) 274; Rintoul M. D. and Torquato S., *Phys. Rev. Lett.*, **77** (1996) 4198.
 - [31] Edwards S. F. and Grinev D. V., *Phys. Rev. Lett.* **82**, 5397 (1999).
 - [32] Leonforte F. *et al.*, *Phys. Rev. B*, **70** 014203 (2004).